MINISTRY OF AVIATION

AERONAUTICAL RESEARCH COUNCIL

CURRENT PAPERS

A Turbine Nozzle Cascade for Cooling Studies Part II. Comparison between Measured and Predicted Mean Nusselt Numbers at the Blade Surface.

by

R. I. Hodge

NATIONAL GAS TURBINE ESTABLISHMENT

A turbine nozzle cascade for cooling studies
Part II   Comparison between measured and predicted
mean Nusselt numbers at the blade surface

- by -

R. I. Hodge

SUMMARY

The condition of the boundary layer around a turbine nozzle blade profile in a two-dimensional cascade is described at various levels of gas flow Reynolds number and turbulence. Mainstream turbulence is shown to have a modifying influence on the accepted transition criteria.

Surface distributions of heat transfer coefficient are calculated for the near isothermal case, with laminar and turbulent boundary layers. Ad hoc experiments are reported which give the blade surface heat transfer coefficients when the boundary layer is separated over part of the convex side.

The combined calculated and estimated values of the profile average heat transfer rate, according to the estimated boundary layer development pattern with flow Reynolds number, are in fair agreement with the measured values quoted in Part I of the present pair of Memoranda.

CONTENTS

APPENDIX

ILLUSTRATIONS

1.0   Introduction

The surface average convective heat transfer coefficients between gas and blade have been measured at various gas conditions in a test cascade installed at this Establishment. The tunnel performance and these heat transfer tests are reported in Part I of the present series of Memoranda.

The opportunity has been taken to test heat transfer prediction methods, by comparing the average of estimated values around the profile with those cascade measurements. The model on which the calculation is based is described in Figure 1.

The details of the estimating procedure are contained in this Memorandum. A comparison between the predictions and the extrapolated experimental results is presented in Figure 17.

2.0   Brief description of the procedure

The calculations were based on the surface pressure distribution obtained with a specially instrumented test blade. From this, the development of a laminar boundary layer extending over the entire blade was calculated, neglecting stability considerations: this yielded the lowest possible value of mean heat transfer coefficient. Also from the same pressure distribution another calculation was made to show the susceptibility of this laminar boundary layer to separate from the blade surface, assuming that prior transition to turbulence did not occur.

Some visualisation techniques were then applied to the test blade, in order to detect the location of turbulent boundary layers at various blade Reynolds numbers: one of these, the lamp-black method, gave clear and reproducible indications on the blade convex side, only affected to a minor degree by length of exposure. These indications however, interpreted as transition points, fell only very approximately into a pattern when compared with the flow Reynolds number. Furthermore this pattern, when interpreted in terms of the boundary layer development parameters of momentum thickness, Reynolds number and pressure gradient factor, exhibited both a level and trend of transition Reynolds number which appeared to be contrary to the results of other experiments. A further complicating feature was therefore suspected: mainstream turbulence levels were measured in the tunnel, were found to vary widely under certain test conditions, and were introduced as a parameter in the transition point plot. At this stage the experimental evidence becomes meagre but a tentative suggestion is made concerning the interaction of the boundary layer parameters and the mainstream turbulence.

The lamp-black indications of transition were extrapolated to the test conditions of the heat transfer measurements of Part I. Nusselt numbers for the turbulent boundary layer at these conditions were then calculated using, by an analogy with skin friction, empirical drag relations.

The extrapolated transition information did not exclude the possibility of separation of the boundary layer from the blade convex side over the low end of the test Reynolds number range. Since there seems to be a dearth of information about heat transfer rates with the boundary layer in this condition, some special experiments were mounted to measure the increase in average Nusselt number with the boundary layer forced into

separation at different stations. This data was then extrapolated to the point of natural separation.

The various calculations, estimates and experimental extrapolations were then combined to give the predicted average heat transfer, valid for a temperature ratio, T_g/T_b , approaching unity, which can be compared with test measurements described in Part I extrapolated to the same value.

3.0 Applicability of the boundary layer heat transfer calculation

The physical properties of air governing the transfer of heat are themselves dependent upon temperature: thus in a thermal boundary layer, where the temperature must vary from the static temperature of the main-stream to that of the surface, these properties must be continuously varied. This phenomenon renders the equations of heat transfer complex. The assumption of temperature-invariant properties simplifies a computation, but obviously introduces errors if the temperature difference is large, unless an effective representative temperature can be selected. An alternative approach is to utilise simplified computation for the case where temperature difference is negligible, but not zero, at some parti-cular gas temperature, t, and to modify the results by a function of the different temperatures, t and T_b for cases in which that difference is not negligible. This latter method is more practical for the purpose of comparing estimate and experiment, and is adopted herein.

A convenient case where the temperature difference is small, in airflow at subsonic velocities, is that of zero heat transfer. Because of viscous dissipation of heat in the boundary layer the temperature pro-file is not uniform, so that the calculation does not become imaginary.

In this case the temperature of the air adjacent to the surface is greater than the static temperature of the mainstream. Pohlhausen (Reference 3, Section 269) has given an approximation for a laminar boundary layer over a flat plate:-

$$T_o = t + Pr^{\frac{1}{2}} \frac{U^2}{2gJc_p} \qquad \dots \dots \quad (1)$$

where T_o is the temperature of the stationary zone adjacent to the surface. Squire (Reference 2, Appendix II) has shown that a similar approximation holds for turbulent boundary layers, with a recovery factor equal to $Pr^{\frac{1}{3}}$. In Reference 4 measured recovery factors have been compared with these approximations; they showed closest agreement when the Prandtl num-ber is evaluated at the temperature T_o.

The expression for T_o can be rewritten in terms of the gas total temperature T_1 and the local Mach number outside the boundary layer, at any point on the surface denoted by the suffix s:-

$$(T_o)_s = T_1 \left\{ 1 - \frac{(1 - Pr^n) \frac{\gamma - 1}{2} M_s^2}{1 + \frac{\gamma - 1}{2} M_s^2} \right\} \dots (2)$$

where the exponent n is either $\frac{1}{2}$ or $\frac{1}{3}$ depending on the nature of the boundary layer.

The calculation is much simplified if the flat plate values of $(T_o)_s$ are accepted for the blade profile, and averaged around the surface. This can be done if conductivity in the airflow direction within the boundary layer is neglected. In the present instance the Mach number variation with chord is substantially linear over the concave surface between the inlet stagnation point and the outlet value, and approximately equal to 1.10 times the outlet value over the convex surface. The average value of $(T_o)_s$ can be adequately represented by

$$(\overline{T}_o)_s \simeq T_1 \left\{ 1 - \frac{0.79(1 - Pr^n) \frac{\gamma - 1}{2} M_2^2}{1 + \frac{\gamma - 1}{2} M_2^2} \right\} \quad \cdots \quad \cdots \quad (3)$$

With the boundary layer completely laminar, taking the Prandtl number for air at $500^\circ K$ $(= 0.67)$

$$(\overline{T}_o)_s \simeq T_1 \left\{ 1 - \frac{0.14 \frac{\gamma - 1}{2} M_2^2}{1 + \frac{\gamma - 1}{2} M_2^2} \right\} \quad \cdots \quad \cdots \quad \cdots \quad (4)$$

If the boundary layer is assumed to be turbulent over half the convex surface only, the numerical factor in the above equation becomes 0.13. The effect of such an alteration is to vary $(\overline{T}_o)_s$ by less than 0.2 per cent T_1.

In the sections that follow the average temperature of the air adjacent to the surface as given in Equation (4) is called the mean effective gas temperature, and written T_g. This is utilised in calculations valid when $\frac{T_g}{T_b} \to 1$, i.e. where the heat transfer (but not the heat transfer coefficient) everywhere is approximately zero.

4.0 Velocity distribution

Boundary layer calculations are based on the momentum equation, the solution of which requires a knowledge of the distribution of velocity just outside the boundary layer. In the present case this velocity pattern was obtained from the measured static pressure at points on the blade surface: a specially instrumented blade replaced the heat transfer blade in the cascade for this purpose.

Figure 2 shows the static pressure distribution around the surface measured[5] at various flow rates: the gas total temperature was about $20^\circ C$ so the condition was a close approximation to the isothermal case. Velocities were calculated from these pressures assuming isentropic expansion. To render the values non-dimensional they were expressed as proportions of the outlet velocity, and are presented in Figure 3. Because of the non-uniform cascade entry velocity distribution, the relevant outlet velocities were deduced by equating the integrated pressure distribution to the rate of change of momentum in the direction perpendicular to that of the blade inlet flow:-

$$\oint_0^X p_s \cos \alpha_s \, dx = \frac{1}{2} \frac{p_2}{R^*_g} s \sin 2\alpha_2 \left(1 + \frac{\gamma - 1}{2} M_2^2 \right) \left(\frac{U_2}{\sqrt{T}} \right)^2 \quad (5)$$

This neglects skin friction which should be subtracted from the static pressure factor on the blade in the perpendicular direction. The magnitude of the skin drag perpendicular component is

$$\left[\int_{0}^{x} \frac{f}{2} \frac{p_s}{R^* g} \sin \alpha_s \left(1 + \frac{\gamma - 1}{2} M_s{}^2\right) \left(\frac{U_s}{\sqrt{T}}\right)^2 \right]_{\text{both surfaces}} \qquad \dots \quad \dots \quad (6)$$

The skin friction was estimated to be less than 1 per cent of the integrated static pressure force.

5.0   Laminar boundary layer calculation

Squires method[2] of laminar boundary layer calculation is based on an approximate solution of the momentum equation which gives the displacement thickness at any point on the blade surface

$$\left(\frac{\delta^*}{c}\right)^2 = \frac{2.96}{R_2} \left(\frac{U_s}{U_2}\right)^{-\epsilon} \int_{0}^{x/c} \left(\frac{U_s}{U_2}\right)^5 d(x/c) \qquad \dots \quad \dots \quad (7)$$

By assuming that the distribution of $\dfrac{T_g - t}{T_g - t_s}$ in the thermal layer is similar to the velocity distribution $\dfrac{u}{U}$ in the momentum layer, and by using the Blasius form in terms of a thermal displacement thickness δ_t, the energy equation for the thermal layer is approximated as follows

$$\left(\frac{\delta_t}{\delta^*}\right)^2 F\left(\frac{\delta_t}{\delta^*}\right) \simeq \frac{0.386}{Pr} \left(\frac{U_s}{U_2}\right)^4 \frac{\displaystyle\int_{0}^{x/c} \left(\frac{U_s}{U_2}\right) d\left(\frac{x}{c}\right)}{\displaystyle\int_{0}^{x/c} \left(\frac{U_s}{U_2}\right)^5 d\left(\frac{x}{c}\right)} \qquad \dots \quad \dots \quad (8)$$

A table of the function $F \dfrac{\delta_t}{\delta^*}$ in Reference 2 enables the ratio $\dfrac{\delta_t}{\delta^*}$ to be deduced from Equation (8): substituting in Equation (7) yields $\delta_{t/c}$. The rate of heat transfer per unit area is the limiting value at the surface of the differentiation of the temperature distribution: this, expressed as a Nusselt number, is

$$(Nu)_s = \frac{0.5715}{\left(\frac{\delta_t}{c}\right)} \qquad \dots \quad \dots \quad \dots \quad \dots \quad \dots \quad \dots \quad (9)$$

Taking the value of Prandtl number as that of air at $500^{\circ}K$ ($= 0.67$), and the velocity distribution as given in Figure 3 for an outlet Mach number $M_2 = 0.55$, Equations (7), (8) and (9) were used to give the distribution of $\dfrac{(Nu)_s}{\sqrt{R_2}}$ shown in Figure 4. The peak value, at leading edge, was taken from an exact solution for the stagnation point on a cylinder given in Reference 3, Section 270. The surface average ordinate, obtained by graphical integration of Figure 4 is 0.549. This is the minimum value $\dfrac{Nu}{\sqrt{R_2}}$ for the test profile, which would result from an entirely laminar boundary layer over the blade surfaces.

5.1   Prediction of laminar boundary layer separation

Separation of the boundary layer occurs when adverse pressure forces cause blocking of the low speed flow in the layer, bringing about a thickening and a consequent deflection of the mainstream away from the surface: this deflection itself modifies the pressure distribution. When a balance is achieved a wake is formed at an origin on the surface, with consequent energy dissipation. The time-average velocity in this wake is approximately zero near the origin, and is in opposition to the mainstream velocity at points downstream.

Stratford[6] has treated the case of laminar separation for the pressure distribution zero from the leading edge to some distance $x' = x'_o$ where an adverse (positive in the direction of the mainstream flow) gradient is initiated. This may be translated into a form with a favourable pressure gradient to the peak suction at a distance x_o from the leading edge, by making x'_o of such a length on a flat plate as to give the same momentum thickness as obtains at the real length x_o. Equation (42) of Reference 6 can be rewritten

$$\frac{x'_o}{c} = \frac{\displaystyle\int_0^{x_o/c} \left(\frac{U_s}{U_2}\right)^5 d\left(\frac{x}{c}\right)}{\left[\frac{(U_s)_{x_o}}{U_2}\right]^5} \qquad \dots \quad \dots \quad (10)$$

By the simultaneous solution of the equations of motion for the outer part of the boundary layer where inertia terms are predominant and for the sublayer where viscous control is exhibited, meeting the requirement of a continuous velocity profile, Stratford derives the approximate Equation (35)

$$\left[C_p \left(x' \frac{\partial C_p}{\partial x'}\right)^2\right]_{sep} = 7.64 \times 10^{-3}$$

where
$$C_p = \frac{p - p_{x'_o}}{\frac{1}{2}\rho U_o^2} \qquad \dots \quad \dots \quad (11)$$

This can be rewritten:-

$$(x'/c)_{sep} = \sqrt{\frac{7.64 \times 10^{-3}}{\left[C_p \left(\frac{\partial C_p}{\partial x'/c}\right)^2\right]_{sep}}} \qquad \dots \quad \dots \quad (12)$$

By plotting (x'/c) obtained from the above equation evaluated at selected (x'/c) points, separation can be predicted when the deduced value equals the selected value.

A full solution, adapted from Equation (41) of Reference 6 is:-

$$(C_p)_{sep} = \sqrt{\frac{7.64 \times 10^{-3}}{\left[x'/c \dfrac{\partial C_p}{\partial x'/c}\right]^2_{sep}}} \left(1 + 0.35\left[\frac{C_p}{x'/c \dfrac{\partial C_p}{\partial x'/c}}\right]_{sep}\right)$$

$$\times \left\{1 + 0.46\left[\frac{C_p \dfrac{\partial^2 C_p}{\partial(x'/c)^2}}{\left(\dfrac{\partial C_p}{\partial x'/c}\right)^2}\right]_{sep} \left(\frac{1 + 0.14\left[\dfrac{C_p}{x'/c \dfrac{\partial C_p}{\partial x'/c}}\right]_{sep}}{1 + 0.8\left[\dfrac{C_p}{x'/c \dfrac{\partial C_p}{\partial x'/c}}\right]_{sep}}\right)\right\}$$

$$\dots \quad \dots \quad (13)$$

this can be solved by an iterative process, but for most practical cases it is sufficient to substitute the approximate values from Equation (12) everywhere except in the first terms of both sides.

The approximate and exact solutions for the present case (velocity distribution as given in Figure 3) are presented in Figure 5. They are given in terms of x/c, the real distance from the blade leading edge which is obtained from the x'/c solutions thus:-

$$x/c = x'/c + (x_o/c - x'_o/c) \quad \dots \quad \dots \quad \dots \quad \dots \quad (14)$$

It will be observed that the approximate solution gives two satisfying values: obviously the downstream value could not exist after the earlier separation. The exact solution corrects this anomaly. The difference between the first approximate solution and the exact one is in this case negligible.

5.1.1 Effect of incidence on separation position

In Part I of the present series the variation of incidence angle across the test blade span is reported; in particular it was observed that at one mode of operation, the outboard section of the blade was operated at about 10° positive incidence. As no velocity distribution around the blade is available for this condition, an estimate was made by comparison between that of the test blade at zero incidence, and the analogue distributions reported in Reference 16, for a similar profile operated at zero and positive incidences.

When that estimated distribution was subjected to the separation criteria, it appeared that separation would occur at $x/c = 0.8$. This value may be compared with $(x/c)_{sep} = 0.84$ deduced for the profile operating at zero incidence, and the conclusion drawn, that positive incidences up to 10° have negligible effect.

6.0   Transition detection

It is known that the boundary layers over turbine blade profiles are not entirely laminar: at some point on one or both surfaces a transition to a turbulent state occurs.   Andrews and Schofield[7] had examined a model having an identical profile to that under consideration here, and found that, with a disturbed entry airflow, transition occurred on the convex surface.   As markedly different heat transfer rates obtain in the two states, it was imperative to have an indication of the position of transition.   Various methods of detection are available but in the present case only two were regarded as practical, i.e. surface total pressure probing and trace methods.

A few trials were attempted with the traversable surface probe shown in Figure 2 of Part I but no conclusive evidence was obtained. Attenuation in the probe prevented detection of the boundary layer noise, and the scatter in total pressure measurement obscured any detail variations.

Several trace methods were also tried: these were

(a)   evaporation of a distillate film from the blade surface,

(b)   removal of a deposit of solid material from the blade surface,

(c)   deposition of a powder on to the blade surface from the airflow.

In the trials of the evaporative technique only liquid distillates were used and the tests were abandoned when it was observed that the films were dragged over the surfaces towards the trailing edge.   It would seem that if a liquid is to be used, surface roughness providing in effect a large number of reservoirs is necessary: alternatively solid volatile films should be used.   The second method proved much more promising, when a deposit of carbon formed from an acetylene-rich flame ("lamp-black") was used as the surface coating.   Repeatable transition indications on the convex side of the profile were observed which were insensitive to test exposure times between 2 and 15 minutes.   On the concave surface however a fairly general thinning of the deposit occurred which was proportional to the duration of the exposure: it was suspected that this was due to the eroding action of the dust load inherent in the airflow.   Applications of the last method were also examined: lycopodium and french chalk were introduced in fluidised form into the airflow some distance upstream from the cascade.   Deposits over the rear of the convex surface were obtained but these were extremely light, even when the surface was rendered sticky.   Lines of demarcation could not be detected, except at the trailing edge where a relatively thick deposit formed rapidly in the wake.

6.1   Transition measurements

The lamp-black method was the best of the transition detection techniques examined: it was easy to use and to interpret, and under identical test conditions gave reproducible results.   Accordingly it was adopted for a general investigation.

(a)   Convex surface

When the results of a survey over the test flow range, using the alternative tunnel compressed air supplies (two different compressors, with and without aftercooling) were examined, wide scatter of the midspan convex side transition points was apparent. The best line through these measurements is shown dotted in Figure 6. This curve is inconsistent with theoretical considerations of laminar boundary layer stability insomuch as indicated transitions upstream of the minimum pressure zone, at high values of the blade Reynolds number, $\frac{U_2 c}{\vartheta_2}$ occur at lower values of the boundary layer parameter, $\frac{U_S \theta}{\vartheta_S}$, than do transitions after the peak velocity point. This fact, coupled with the scatter which was extreme compared with the reproducibility of the initial trials, suggested that a further complicating feature was involved. It was suspected that turbulence in the entry airflow was this feature.

(b)   Concave surface

At low velocity flows the lamp-black coating appeared to be removed from the concave surface more rapidly nearer the trailing edge, but no distinctive change could be detected. At higher blade Reynolds numbers the rate of removal from this surface was fast and exposures had to be limited to under one minute for any trace to be left. Such tests were unsatisfactory, and merely suggested that there might be a transition at about $x/c = 0.8$.

6.2   Turbulence measurements

Prototype equipment, as described in Reference 8, was installed in the tunnel and used to survey the turbulence levels obtaining with the various compressed air facilities in use, and also under the conditions of the heat transfer measurements of Part I, i.e. with combustion. The measurements were made $\frac{1}{2}$ chord upstream from the leading edge of the test blade, at midspan. The sensory head of this equipment is a glass wedge with a thin deposited coating of platinum forming an arm of the detector bridge circuit. With the apex of the wedge pointing upstream, velocity perturbations in the direction of the mainstream are sensed. Associated integrating equipment gave readings which after calibration, could be interpreted as the square root of the average of the squares of the instantaneous velocities

The results of the survey are given in Figure 18 where the ratio of the stream-direction r.m.s. velocity perturbation to mainstream velocity is plotted against blade outlet Reynolds number. Considerable scatter is apparent in the runs with combustion, but this is not attributable to particular selections of compressor or combustion temperature rise, and indeed a varying dial reading was observed during each particular test.

6.3   Transition criteria

Fully developed turbulence appears in the boundary layer some distance downstream from the limit of stability of laminar flow: a delay length occurs depending upon the amplification of disturbances appearing in the zone of instability. The limit of stability of the laminar boundary layer is reached when disturbances introduced into or originating within the boundary layer are no longer damped out.

A number of investigators have studied these pheomena, with parti-
cular reference to the conditions obtaining on the surface of aircraft
wings. Crabtree[9] has given a critical survey of their findings and
shows how various experimental measurements of transition can be recon-
ciled against the parameters

(a)   boundary layer Reynolds ratio, $\dfrac{U_s\theta}{\vartheta}$

(b)   impressed pressure gradient factor, $\dfrac{\theta^2}{\vartheta}\dfrac{dU_s}{dx}$

The reciprocal of the first parameter is a measure of the damping present,
and negative values of the second give the available amplification.
Under the conditions of Crabtree's study, $\left(\dfrac{(u)_{r.m.s.}}{U} = 0.1 \text{ to } 0.2 \text{ per}\right.$
$\left.\text{cent}\right)$, the boundary layer Reynolds number permitting instabilities to
develop range from 1300 to about 750 for amplification factors 0 to 0.09
i.e. for pressure gradients as obtain on a flat plate to values suffi-
ciently severe to cause laminar flow separation. Under favourable pres-
sure gradients the damping has to be very small before transition occurs,
for example at $\dfrac{\theta^2}{\vartheta}\dfrac{dU_s}{dx} = +0.01$ the boundary layer Reynolds
number = 2,200.

When the free stream turbulence is sufficiently high it seems fair
to assume that the appearance of transition will be more dependent upon
the inability of the damping mechanism in the boundary layer to cope with
the introduced disturbances than upon the amplification of comparatively
negligible perturbations. Thus it is to be expected that large scale
turbulence will bring about transition above a certain critical Reynolds
number irrespective of the value of positive pressure gradients up to the
limit where separation occurs: large negative pressure gradients, which
are disturbance-reducing by nature will supplement the boundary layer
damping and should increase the critical momentum thickness Reynolds
number.

When turbulence is introduced as a parameter in the lamp-black
investigations the family of lines shown solid in Figure 6 can be con-
structed. The points about these lines have been transposed to a map of
boundary layer Reynolds number against pressure gradient parameter in
Figure 7. This field was constructed for various blade outlet Reynolds
numbers, from the velocity distribution for $M_2 = 0.55$ given in Figure 3.
Unfortunately most of the data is closely grouped when examined in this
way, and only the 2 per cent turbulence points can be construed in
support of the present hypothesis that the amplification factor is an
unimportant variable in the presence of high mainstream turbulence.

The concave side of the blade operates under large positive pres-
sure gradients. If the suspected transition at $x/c = 0.8$ for blade
Reynolds numbers greater than about 6×10^8 is accepted, this suggests
that the 4 per cent turbulence curve rises steeply, as shown in Figure 8.
Some support for this suggestion was obtained by mounting a special heat
transfer test: a boundary layer trip (of the type described later in
Section 8.1) was attached to the concave surface at $x/c = 0.8$ where it
was expected to cause transition if this did not already occur; the
test showed that heat transfer coefficients greater than normal were
obtained up to $R_2 = 8 \times 10^5$. This was interpreted to indicate that
transition there occurred at that flow, and the point is shown in Figure 8.

The results of these tests, freely extrapolated, are shown in Figure 9. The results of the other investigators, as compiled by Crabtree in Reference 9, and additionally a curve attributed to Schlichting taken from Reference 10, are included for comparison. The present test points are compatible with Crabtree's curve, but not with the earlier German work: in particular very low critical Reynolds numbers ($\simeq 10^2$) at small negative pressure gradient factors (-0.02) would require transition very near the minimum pressure point at blade Reynolds numbers as low as 7×10^4, a phenomenon which was certainly not indicated by the lamp-black technique.

6.4 Corrected transition data

The turbulence level under the conditions of the heat transfer tests does not vary much from 4 per cent over the flow range examined: it was further assumed that this uniformity would extend over the entire test flow range. Transition points as indicated on Figures 7 and 8 for the extrapolated 4 per cent turbulence curve were therefore expected to apply. This corrected pattern is given in Figure 10.

7.0 Turbulent boundary layer calculations

The heat transfer coefficients under the turbulent boundary layers may be obtained, as suggested by Squire[2], from the Kármán generalisation of Reynolds analogy:-

$$Nu_s = \frac{R_2 \, U_s/U_2}{F_1(z,Pr)} \quad \ldots \quad \ldots \quad \ldots \quad \ldots \quad \ldots \quad \ldots \quad (15)$$

$$\text{where} \quad z = \sqrt{\frac{\rho U_s^2}{\tau_0}}$$

$$\text{and} \quad F(z,Pr) = \frac{z}{Pr}\left[z + 5\left\{ (Pr - 1) + \ell n\left(\frac{5Pr + 1}{6}\right)\right\} \right]$$

Squire and Young (Appendix I, Reference 11) develop Kármán's formula for local surface friction on a flat plate to give the empirical relation:-

$$\frac{U_s}{\vartheta} = 0.2454 \, e^{0.3914\,z} \quad \ldots \quad \ldots \quad \ldots \quad \ldots \quad \ldots \quad (16)$$

By substitution in the boundary layer momentum equation, assuming $\frac{\delta^*}{\theta} = 1.4$, they obtain

$$\frac{dz}{dx} + 6.13 \frac{1}{U_s} \frac{\delta U_s}{dx} = \frac{U_s}{\nu} F_2(z) \quad \ldots \quad \ldots \quad \ldots \quad \ldots \quad \ldots \quad (17)$$

$$\text{where} \quad F_2(z) = \frac{10.411 \, e^{-0.3914\,z}}{z^2} \quad \ldots \quad \ldots \quad \ldots \quad \ldots \quad \ldots \quad (18)$$

Equation (17) may be solved by an iterative method from the transition position, at which point the initial value of z is calculated from Equation (15) taking the momentum thickness θ there from the earlier laminar boundary layer calculation. Substitution of local values of z in Equation (15) gives the required Nusselt number distribution.

This method was used to estimate the heat transfer coefficients at x/c intervals of 0.05 from transitions at $x/c = 0.5$ to 1.0 at intervals of 0.1 on the convex side, at blade Reynolds numbers $R_2 = 5$, 7 and 9×10^5, and similarly from transitions at 0.6 to 0.8 at R_2 values of 5 and 9×10^5 on the concave surface. The Prandtl number for air at $500°K$ was introduced in Equation (15). The distributions, superimposed on the basic laminar flow pattern, are given in Figure 11. The combination of rapidly increasing U_S/U_2 with relatively small increase in $\theta_{laminar}$ on the concave side causes increase in Nu_S at the transition point as that point moves towards the T.E., whereas the $U_S/U_2 - \theta_{laminar}$ combination over the downstream half of the convex surface results in a diminishing transition point value.

8.0 Heat transfer under a separated boundary layer

The calculation in Section 5.1 indicates that the laminar boundary layer will separate at $x/c = 0.84$ from the blade convex surface. The lamp-black tests under low turbulence conditions suggest that transition to turbulence occurs first at about this value, at $R_2 \simeq 5 \times 10^5$; while these tests do not give visualisation of separation phenomena they do not invalidate their assumption for Reynolds numbers below 5×10^5. The fluidised powder tests, under similar low turbulence conditions and at low Reynolds numbers, gave slight detectable traces over approximately the last quarter of the convex surface: this could be construed as an indication that separation had occurred.

As long as the history of the boundary layer is entirely laminar, the considerations in the separation calculation in Section 5.1 remain valid, irrespective of the level of turbulence in the mainstream. The argument in Section 6.3 postulates that, under the turbulent conditions of the heat transfer investigation, the convex side boundary layer does remain laminar for values of $\dfrac{U_S \theta}{\vartheta}$ below about 380. This figure is reached at $x/c = 0.84$, at a blade Reynolds number $\simeq 2.8 \times 10^5$. It is therefore assumed that separation occurs at $x/c = 0.84$ up to this value, as described in Figure 10.

There is reason to suppose that heat transfer coefficients under separated laminar boundary layers will be very small: the theoretical analysis in Reference 12 suggests that they should be about half that of the attached laminar layer, in air at subsonic velocities. However very high values have been observed under experimental conditions where separation of a laminar layer can be reasonably supposed: for example the measurements on a blade profile in cascade reported by Wilson and Pope[13], and on the walls of a tube after an abrupt diameter enlargement as described in Reference 14.

A separated laminar layer is unstable in subsonic flow: von Doenhoff's experiments[15] indicate that transition, in the separated state, will occur after a very short distance, given by assuming a critical Reynolds number $\dfrac{U_S(x - x_0)}{\vartheta}$ of about 5×10^4. Under the present test

conditions at the limit of separated flow this would require a length along the blade surface of $\Delta x/c \simeq 0.2$. However this figure is probably large in view of the high level of turbulence: there is no known basis for estimating the perseverence of the separated laminar layer under such conditions. For the present purpose it is assumed that transition occurs immediately after separation, and that the relevant heat transfer coefficients are experienced from that point.

The mechanism of heat transfer under separated turbulent boundary layers has not been fully explored. Chapman[12] applies a theoretical velocity spread at $M = 0$ and experimental values at $M = 1.6$, to give heat transfer coefficients in the ratio 6.3/1 and 2.8/1, respectively, to those obtaining under an attached turbulent boundary layer. Very approximately the values quoted in References 13 and 14 may be construed as giving ratios of about 2 and 2.2 respectively, for subsonic velocities. Further data are obviously required, so it was decided to resort to ad hoc experimentation in the present case.

8.1   Heat transfer measurements with tripped boundary layer

As stated earlier, it was suspected that the test blade operated with a laminar boundary layer separating at $x/c = 0.84$ on the convex side, up to a blade Reynolds number $= 2.8 \times 10^5$. To get a measure of the heat input due to separation it was necessary to create separation at known points upstream of the natural position. Small spanwise protuberances from the surface seemed likely to cause such separation. A large step would obviously give rise to a wake and produce an unnatural boundary layer development, so it was decided to limit the height of the trip to below that of the estimated displacement thickness of the laminar boundary layer. To promote separation rather than attached turbulence, these trips were not used upstream of the peak velocity point on the profile.

Two convex side positions were chosen, at $x/c = 0.6$ and 0.7 respectively. The estimated displacement thickness is shown in Figure 12: to keep below this at the upstream positions at $R_2 = 4 \times 10^5$, a maximum trip height $= 0.003$ in. could be accommodated. Accordingly trips 0.003 in. $\times 0.006$ in. chordwise width were built up on the blade surface. This was done by forming a channel between two strips of cellulose adhesive tape placed spanwise on the blade surface and separated by 0.006 in.; a polyester resin cement was poured into the channel so formed and scraped level with the surface of the adhesive strips; when the cement had hardened the strips could be washed off with solvent, leaving a rectangular-sectioned barrier on the blade surface.

The modified blades were examined over a range of Reynolds number (R_2) using the lamp-black visualisation technique. In each case the coating remained untouched up to the Reynolds number where previously a transition had been indicated at the trip position. This supported the assumption that separation was being brought about as planned.

Total heat flow measurements were made on the modified blades over a range of Reynolds number R_2 and temperature ratio T_g/T_b as described for the basic tests in Part I. The extrapolated curves for $T_g/T_b = 1$ are presented in Figure 13a. By taking readings of Nu from these curves at various Reynolds numbers and subtracting from them the calculated average Nusselt number for entirely laminar flow, $(\overline{Nu})_{lam.}$, the increment in the average heat transfer coefficient due to the separated flow could be obtained. Multiplying this increment $\Delta\overline{Nu}$ by the ratio of the total

blade surface to the surface under the separated flow, $\dfrac{S_g}{x_{te} - x_{sep}}$, gave the average heat transfer coefficient obtaining over the last section of the convex surface. These values are presented in Figure 14. The fact that the lines joining the two test points at each Reynolds number when extrapolated to the TE are approximately straight indicates that the local coefficients do not vary greatly. Estimated patterns for the two trip positions are given in Figure 15.

In Section 6.3 a test is mentioned which confirmed that transition to turbulence occurred on the concave side at x/c = 0.8, at Reynolds number R_2 = 8 × 10^5. In this test the blade was modified by the addition of a trip at the point in question. Figure 12 demonstrates that in this case the trip did not protrude beyond the boundary layer displacement thickness within the test range. Lamp-black tests indicated that transition did definitely occur above R_2 = 7 × 10^5. The heat transfer results are given in Figure 13b, showing that the trip loses its influence at R_2 = 8 × 10^5, suggesting that transition occurred at that flow and position on the original blade.

9.0 Combined results

The basic laminar flow relationship gives a mean value over the profile $\dfrac{(Nu)_{laminar}}{\sqrt{R_2}}$ = 0.549. The calculated increments to the basic profile average Nusselt number due to transition at various points on the convex side are plotted in Figure 16a. Those due to turbulence from various positions on the concave side are given in Figure 16b. The difference between the measured values with separated flow on the convex side and the calculated laminar average are presented in Figure 16c: an extrapolated value obtained from the plot on Figure 14 for the calculated separation point x/c = 0.84 is included.

The calculated average Nusselt numbers over the test range can then be obtained by the addition of the increments to the basic relation, according to the boundary layer behaviour pattern of Figure 10. The combined results are presented in Figure 17, where they may be compared with the test results abstracted from Part I. The agreement is good over the low end of the flow range, up to R_2 = 5 × 10^5. Above this the calculated results are rather high, the maximum error being about 10 per cent at R_2 = 7 × 10^5 and upwards.

10.0 Conclusions

Insomuch as the profile average value is a guide, the methods of prediction of point heat transfer coefficients seem adequate: the possibility of various errors which when combined cancel out cannot however be excluded. It should be noted that the condition of the boundary layer is an important factor in the determination of the blade surface average heat transfer coefficient; variation of the point at which the laminar flow breaks down can materially affect this average value, as can the nature of the break down (separation or transition). Thus in an estimate of average heat transfer coefficient, accurate knowledge of the boundary layer development is essential.

If the assumptions are valid, it may be concluded that separated flow is a more forceful heat transfer process than attached turbulent flow: for example, at a Reynolds number of 5 × 10^5 the local values of Nusselt number are much the same at the initiation of either separation

or transition, but after development of the relevant boundary layer state to the trailing edge the seperated flow gives point heat transfer coefficients between 60 and 80 per cent greater than obtain under an attached turbulent boundary layer.

Accepted methods of predicting transitions do not make reference to the mainstream turbulence level. This parameter is included in a suggested relationship between the conventional criteria given in Figure 9.

ACKNOWLEDGEMENTS

REFERENCES

No.	Author(s)	Title, etc.
1	R. I. Hodge	A turbine nozzle cascade for cooling studies. Part I The measurement of mean Nusselt numbers at the blade surface. C.P.492. 1958.
2	H. B. Squire	Heat transfer calculation for aerofoils. A.R.C. R. & M. No. 1986, 1942.
3	S. Goldstein (Editor)	Modern developments in fluid dynamics. Oxford University Press, 1938.
4	L. M. Mack	An experimental determination of the temperature recovery factor (Jet Propulsion Laboratory, California Institute of Technology). Report No. 20-80, August, 1954.
5	H. Ogden	Unpublished test measurements at N.G.T.E.
6	B. S. Stratford	Flow in the laminar boundary layer near separation. A.R.C. R. & M. 3002, 1957.
7	S. J. Andrews N. W. Schofield	An experimental investigation of a thick aerofoil nozzle cascade. A.R.C. 13.632. May, 1950.
8	S. C. Ling	Measurement of flow characteristics by the hot film technique. State University of Iowa, Pub. No. 12,905, 1955.
9	L. F. Crabtree	Prediction of transition in the boundary layer on an aerofoil. A.R.C. 19.310. 1957.
10	A. Walz	Naherungsverfahren zur Berechnung der laminaren und turbulenten Reibungsschicht Deutsche Luftfahrtforschung. U.M. Nr.3060, 1943.
11	H. B. Squire A. D. Young	The calculation of the profile drag of aerofoils. A.R.C. R. & M. No. 1838, 1937.
12	D. R. Chapman	A theoretical analysis of heat transfer in regions of separated flow. N.A.C.A. T.N. No. 3792, 1956.
13	D. G. Wilson J. A. Pope	Convective heat transfer to gas turbine blade surfaces. Proc. I.Mech.E. Vol. 168, No. 36, 1952.

REFERENCES (cont'd)

No.	Author(s)	Title, etc.
14	A. J. Ede C. I. Hislop R. Morris	Effect on the local heat-transfer coefficient in a pipe of an abrupt disturbance of the fluid flow: abrupt convergence and divergence of diameter ratio 2/1. Proc. I. Mech. E. Vol. 170, No. 38, 1956.
15	A. E. von Doenhoff	A preliminary investigation of boundary layer transition along a flat plate with adverse pressure gradient. N.A.C.A. TN.639, 1938.
16	T. J. Hargest	The theoretical pressure distribution around some conventional turbine blades in cascade. A.R.C. 13.360. 1950.

APPENDIX I

NOTATION

c	blade chord
c_p	specific heat at constant pressure
C_p	pressure coefficient defined in the text
f	coefficient of friction at blade surface
g	gravitational constant
M	Mach number at a point locality
n	Prandtl number exponent in temperature recovery equation
Nu	Nusselt number at a point locality
$\overline{Nu}$	Nusselt number averaged around the profile
$\Delta\overline{Nu}$	difference between two profile average Nusselt numbers
p	static pressure
Pr	Prandtl number
R^*	gas constant (taken at the value for air)
R_2	Reynolds number defined in terms of mass flow and outlet dimensions, blade chord, and absolute viscosity measured at the effective temperature of the gas
s	blade pitch
S_g	profile perimeter
t	gas static temperature
T, T_1, T_0	gas total temperatures
T_g	gas effective temperature
T_b	blade surface temperature
u	velocity in mainstream direction at a point within the boundary layer
$(u)_{r.m.s.}$	root mean square perturbation velocity in the mainstream direction
x	surface length measured from LE to a point on the profile
x'	surface length measured from the LE of an equivalent flat plate entry to a point on the profile downstream of the pressure minimum on the convex side

APPENDIX I (cont'd)

z	defined in the text
α	gas angle measured from the perpendicular to the blade pitch
γ	ratio of the specific heats
δ^*	boundary layer displacement thickness
δ_t	boundary layer thermal displacement thickness
θ	boundary layer momentum thickness
ϑ	gas kinematic viscosity
ρ	gas density
τ	boundary layer shear stress

Positional suffices

1	blade row inlet
2	blade row outlet
o	adjacent to the wall within the boundary layer
s	on the profile perimeter
sep.	at the separation point
te	over the length between leading and trailing edges
x'	over the length measured from the equivalent flat plate leading edge

FIG.I.
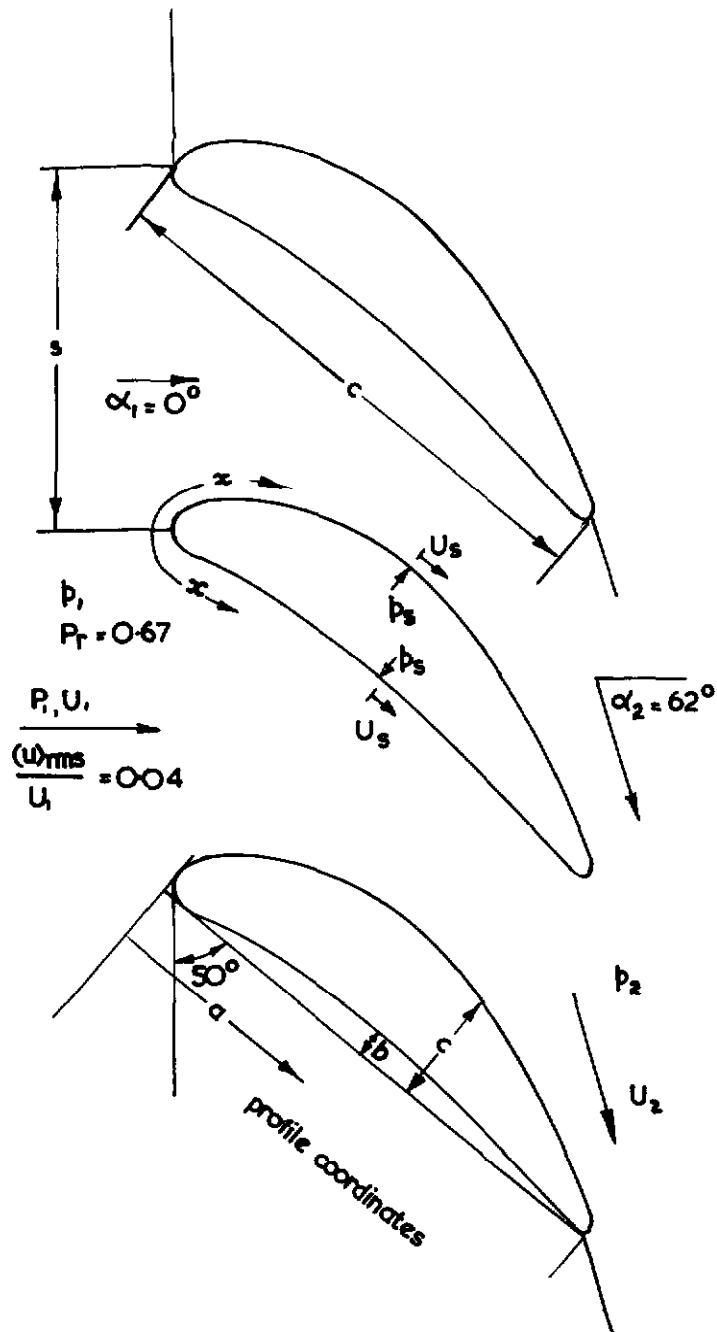
a	O	·054	·108	·162	·216	·324	·432	·648	·864	1·08	1·296	1·512	1·728	1·944	2·054	2·162
b	·030	·006	·012	·022	·032	·057	·077	·102	·113	·111	·102	·090	·070	·037	·020	O
c	·030	·130	·190	·234	·271	·327	·370	·420	·428	·412	·370	·303	·216	·115	·058	·05

CASCADE GEOMETRY

FIG. 2.
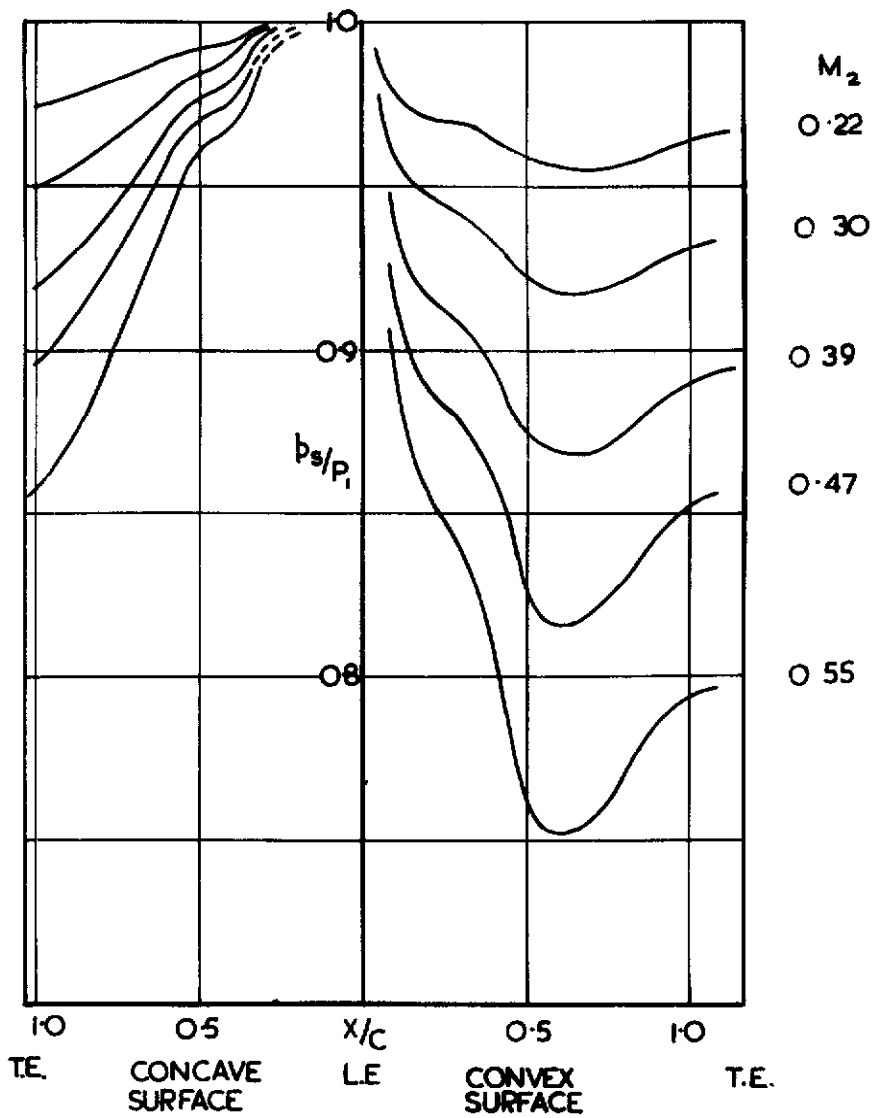
SURFACE STATIC PRESSURE DISTRIBUTION

FIG.3.
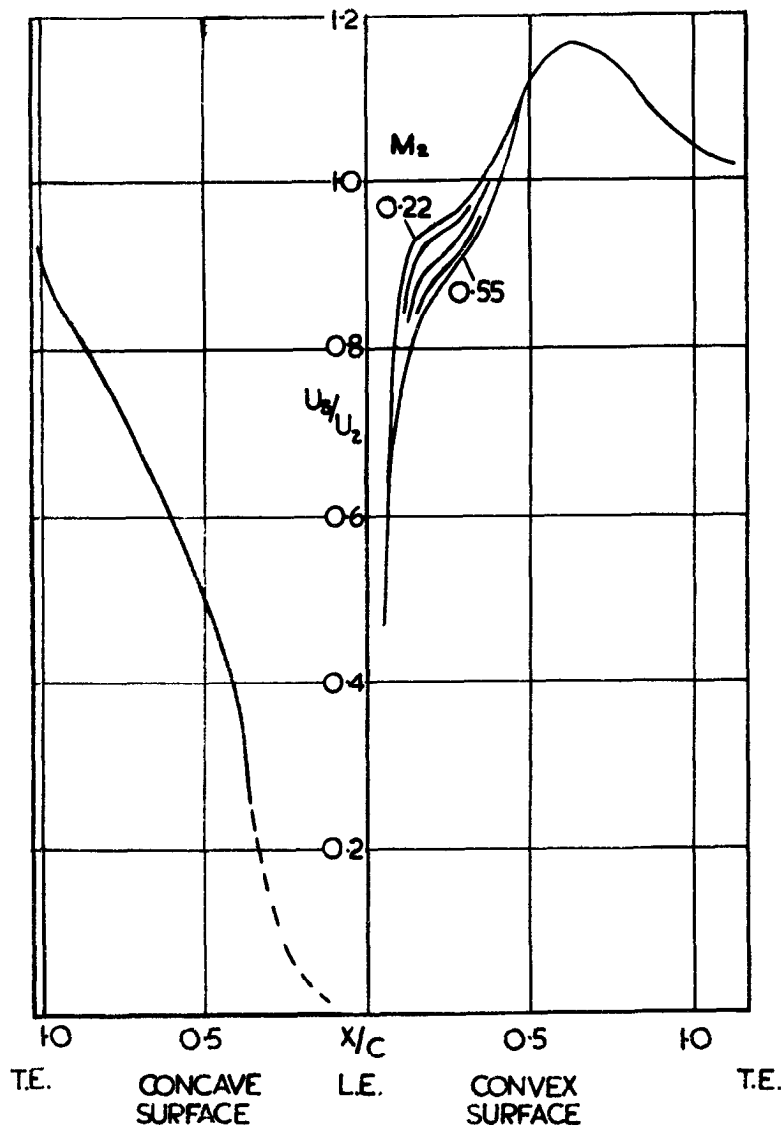
SURFACE VELOCITY DISTRIBUTION

FIG.4.
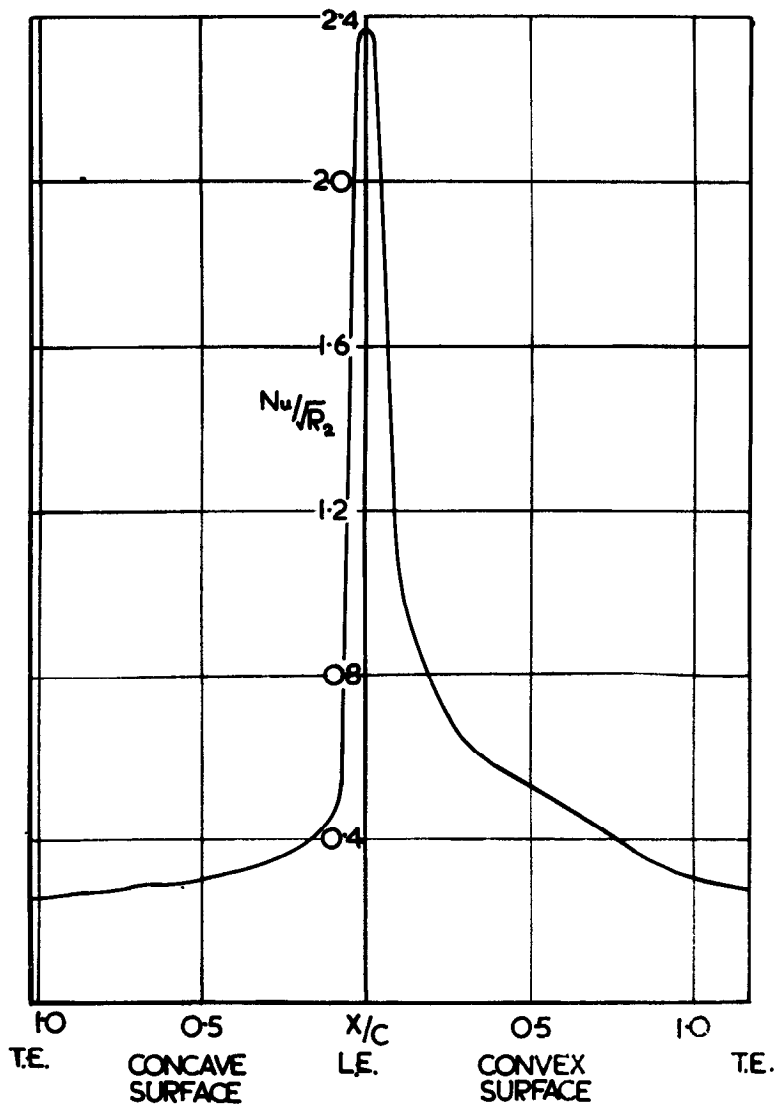
CALCULATED HEAT TRANSFER UNDER A LAMINAR
BOUNDARY LAYER
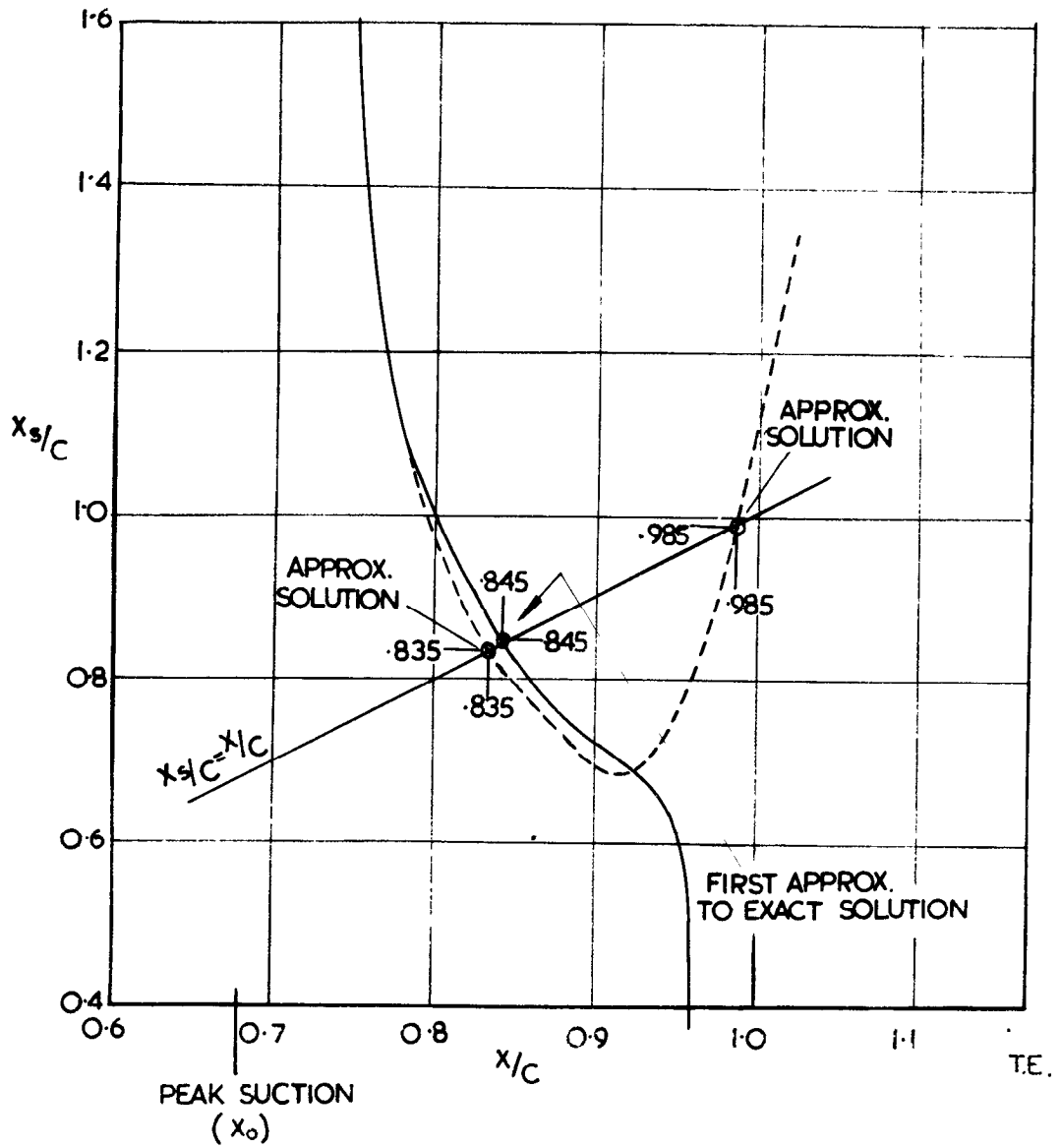
SEPARATION POSITION CALCULATION

FIG. 5.
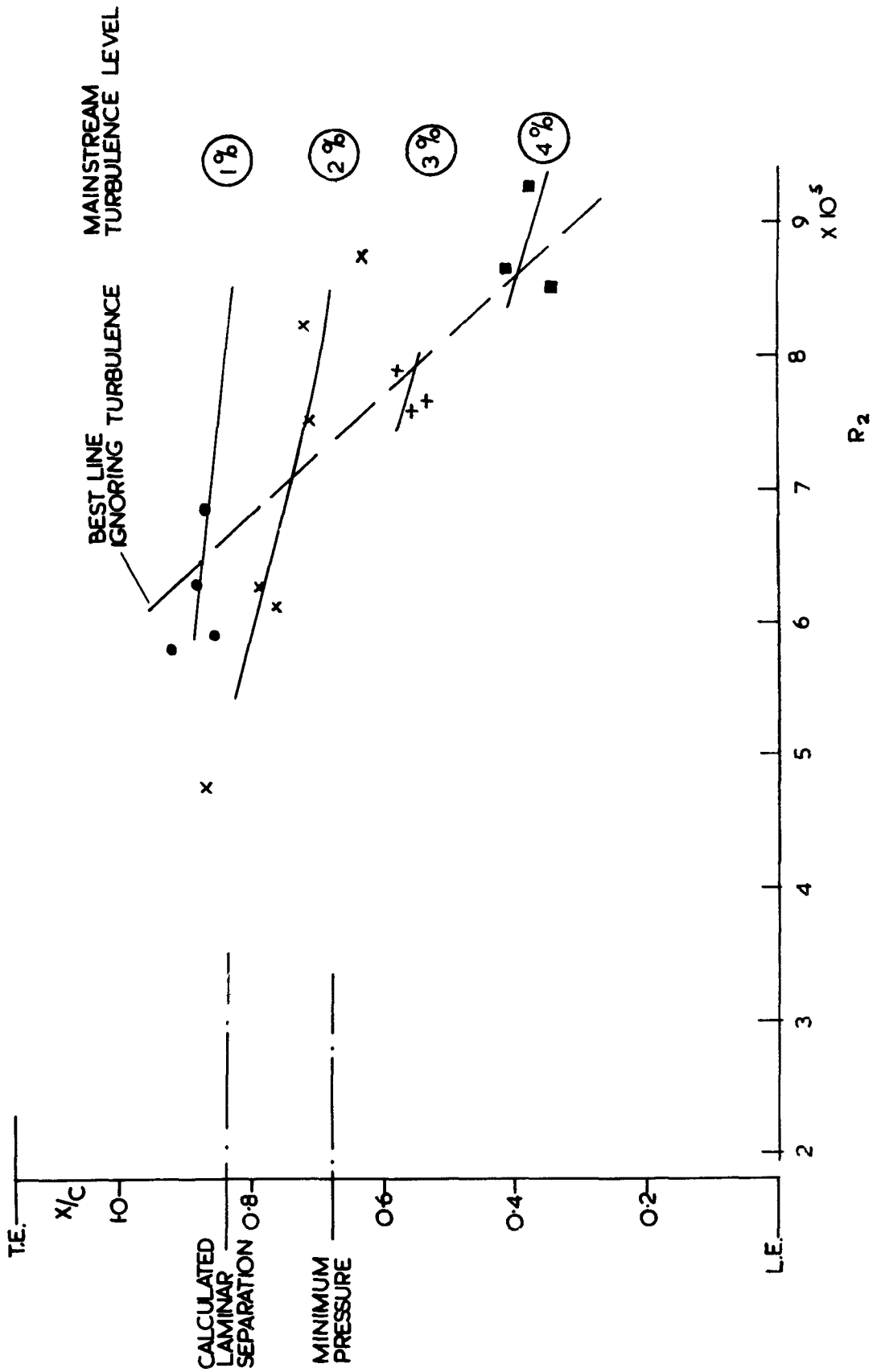
FIG. 6.

INDICATED TRANSITION ON CONVEX SIDE

FIG. 7.
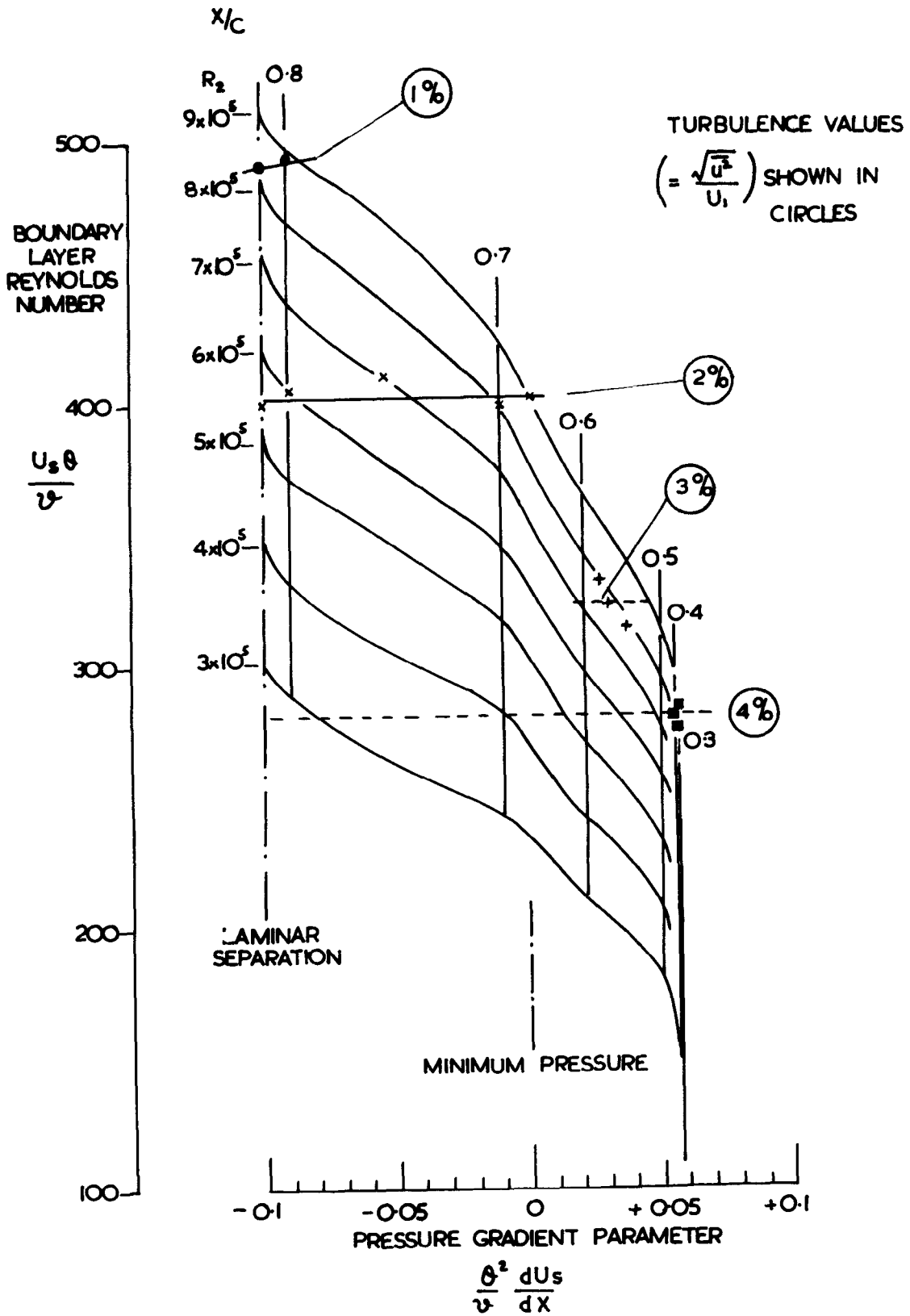
INDICATED TRANSITION COMPARED WITH BOUNDARY
LAYER STABILITY PARAMETERS
(CONVEX SIDE)

FIG. 8.
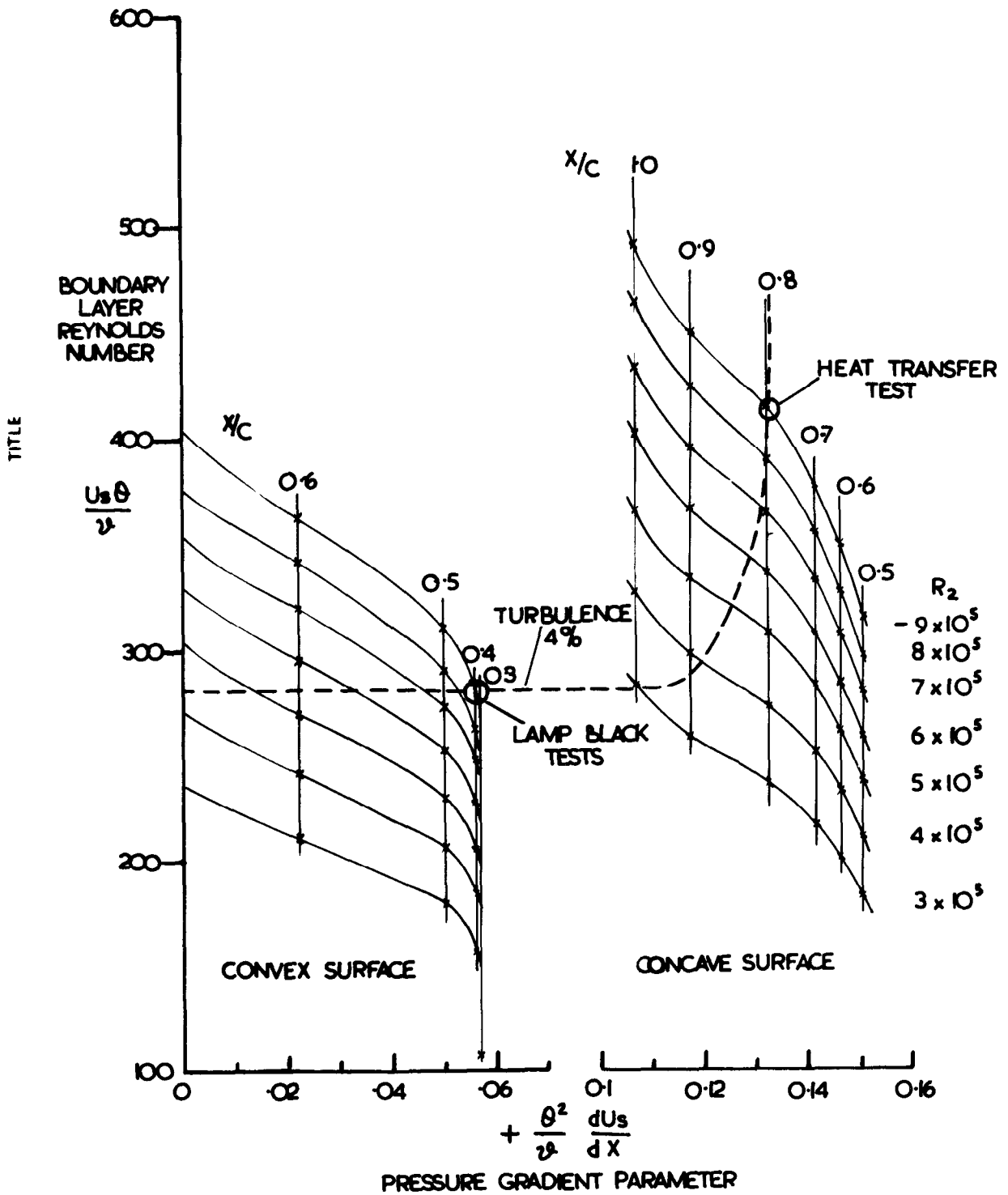
INDICATED TRANSITION COMPARED WITH BOUNDARY
LAYER STABILITY PARAMETERS
(CONCAVE SIDE)

FIG. 9.
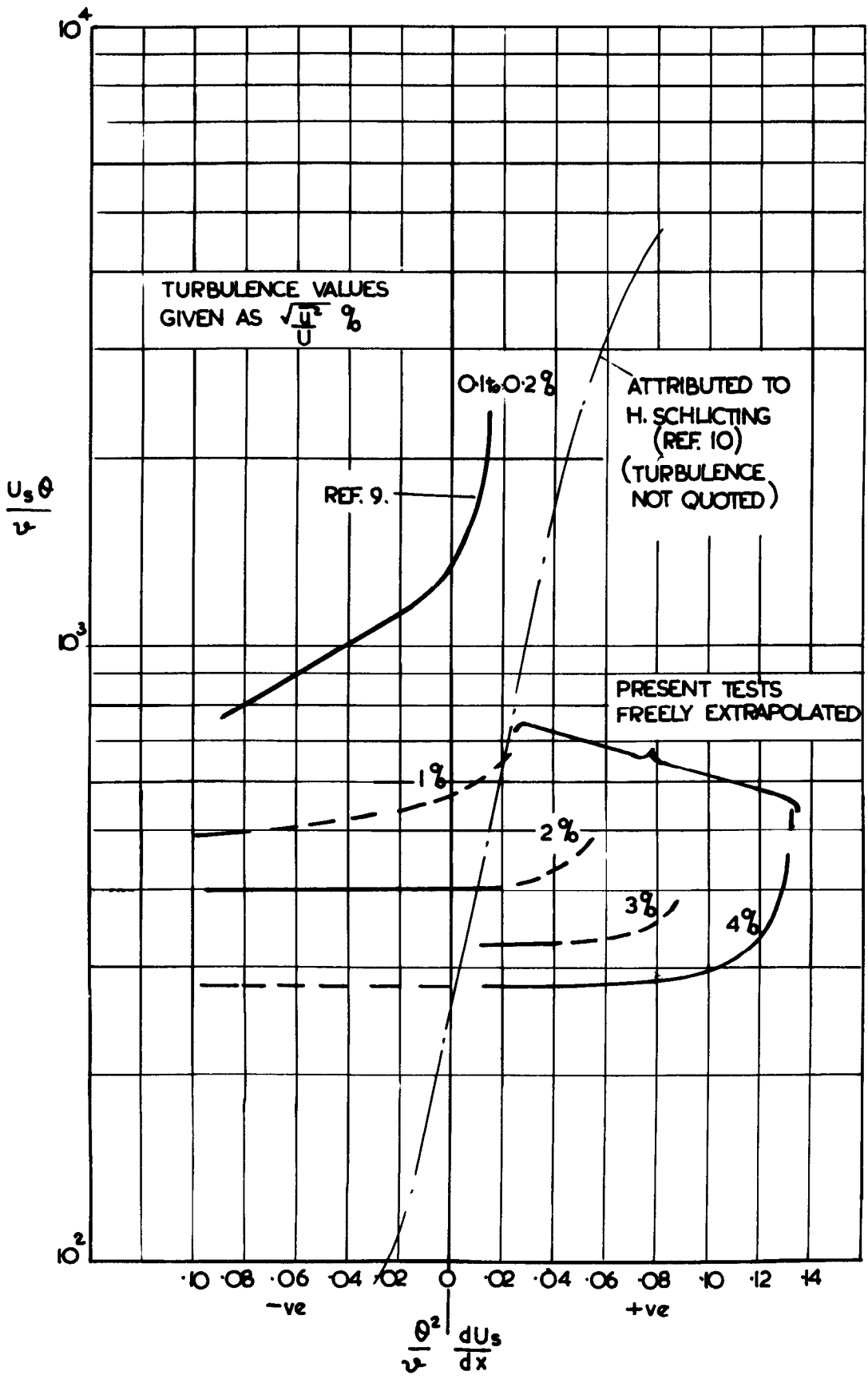
SUGGESTED EFFECT OF MAINSTREAM TURBULENCE
ON TRANSITION CRITERIA
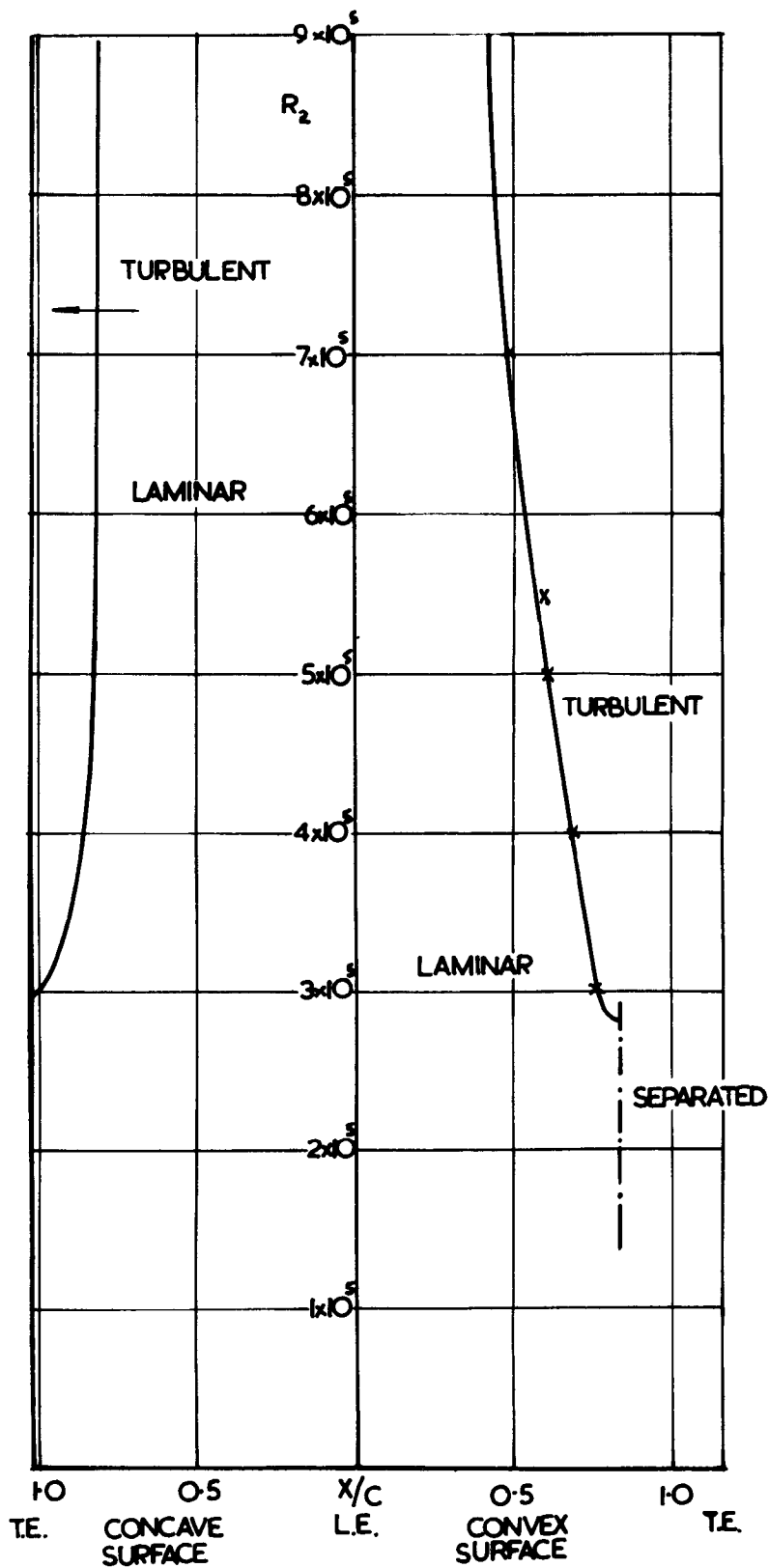
CORRECTED TRANSITION ON BOTH SURFACES

FIG. II.

$R_2 = 5 \times 10^5$

$R_2 = 7 \times 10^5$

$R_2 = 9 \times 10^5$
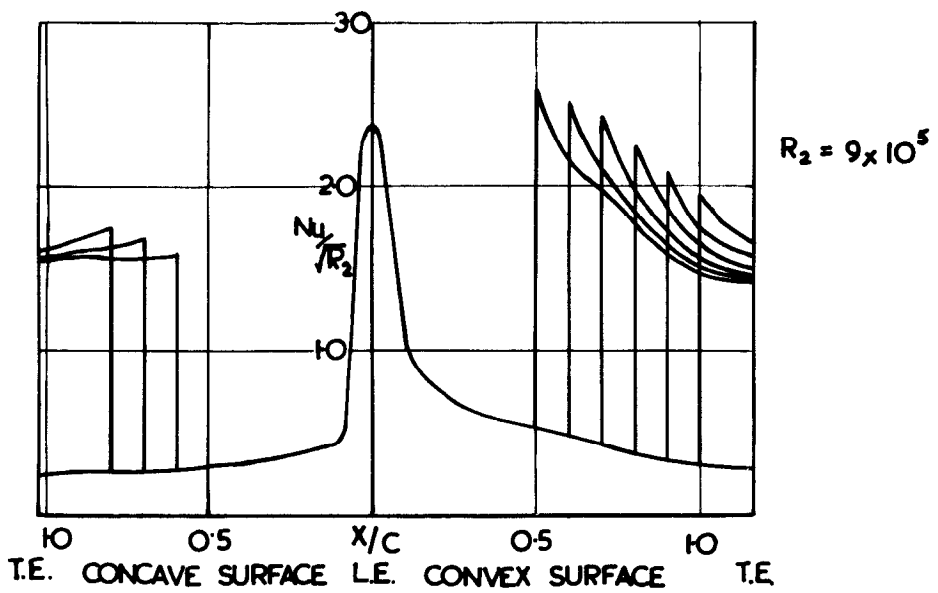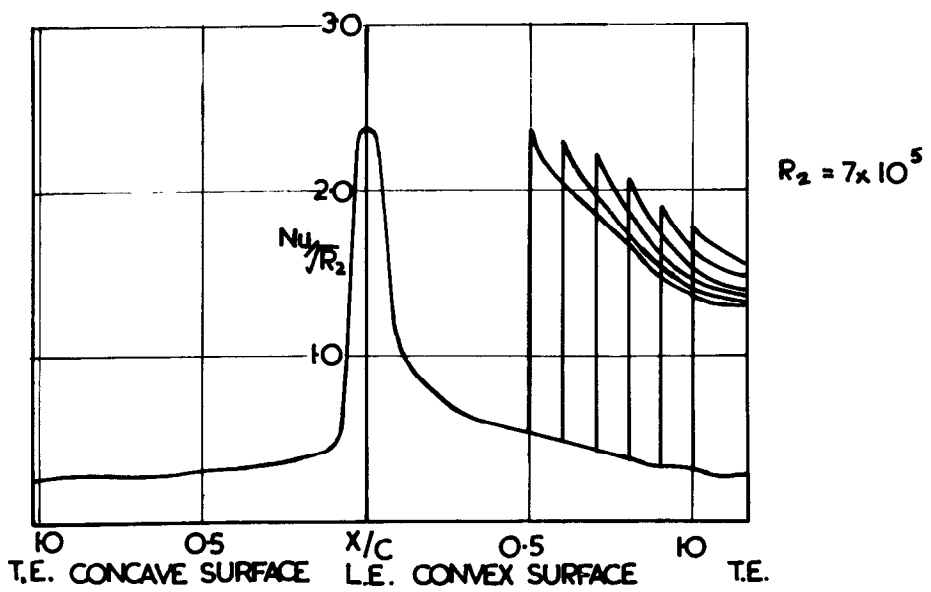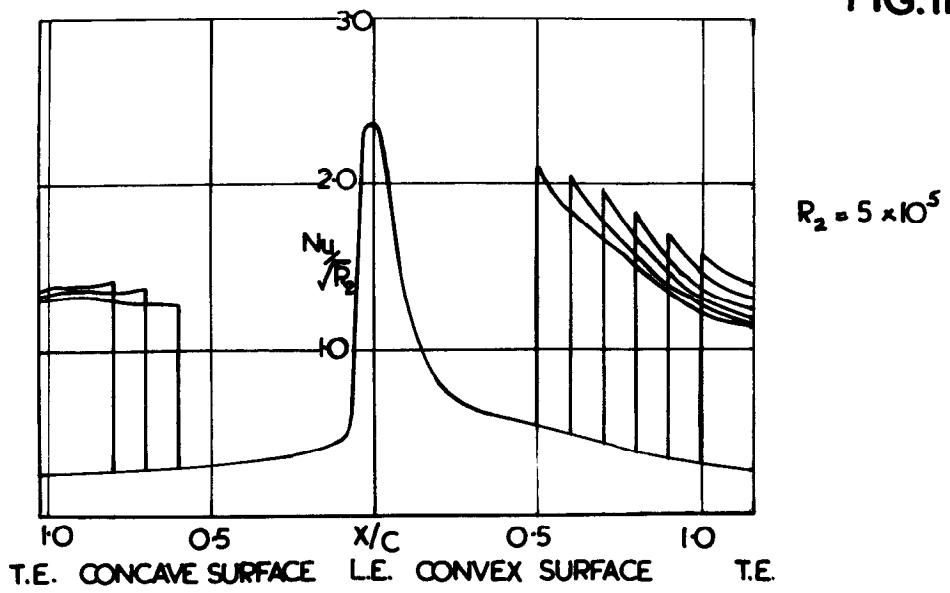
CALCULATED HEAT TRANSFER WITH ARBITRARY
TRANSITION

FIG. 12.
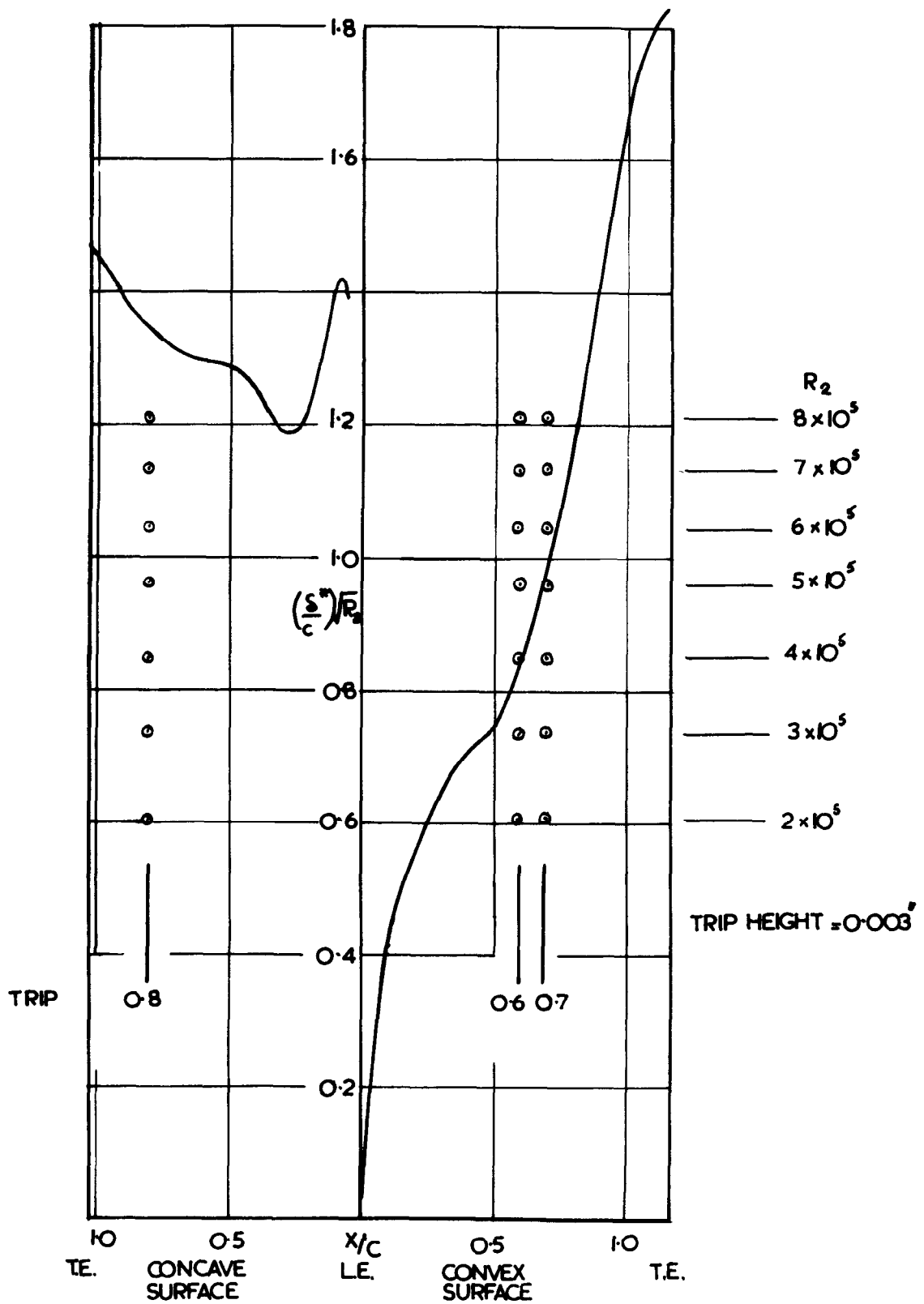
HEIGHT OF BOUNDARY LAYER TRIP COMPARED WITH
BOUNDARY LAYER DISPLACEMENT THICKNESS

FIG. 13.

a) CONVEX SIDE

$\bar{N}u$, R_2, TRIP 06 07, NORMAL

b) CONCAVE SIDE

$\bar{N}u$, R_2, TRIP 08, NORMAL
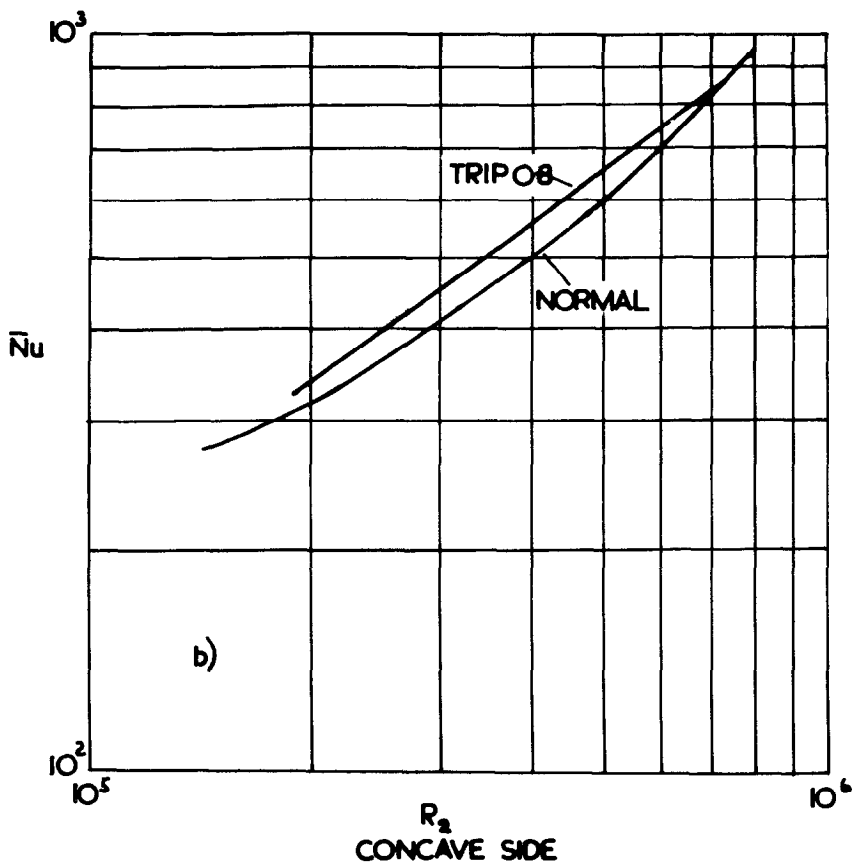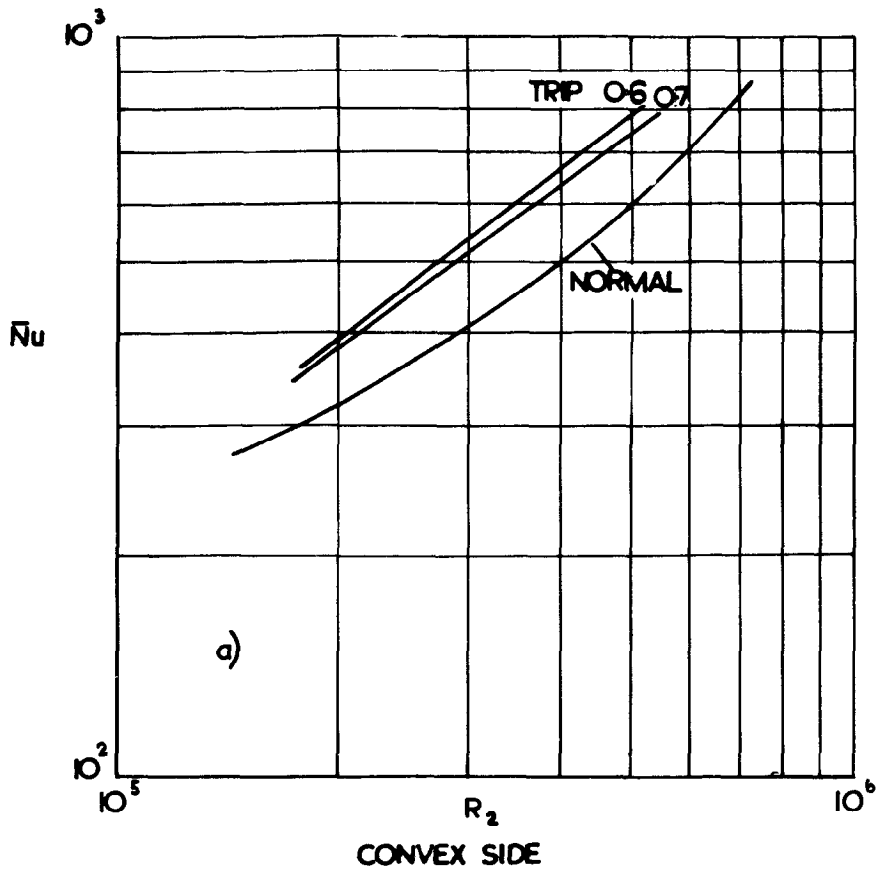
HEAT TRANSFER MEASUREMENTS ON MODIFIED BLADE

FIG. 14.
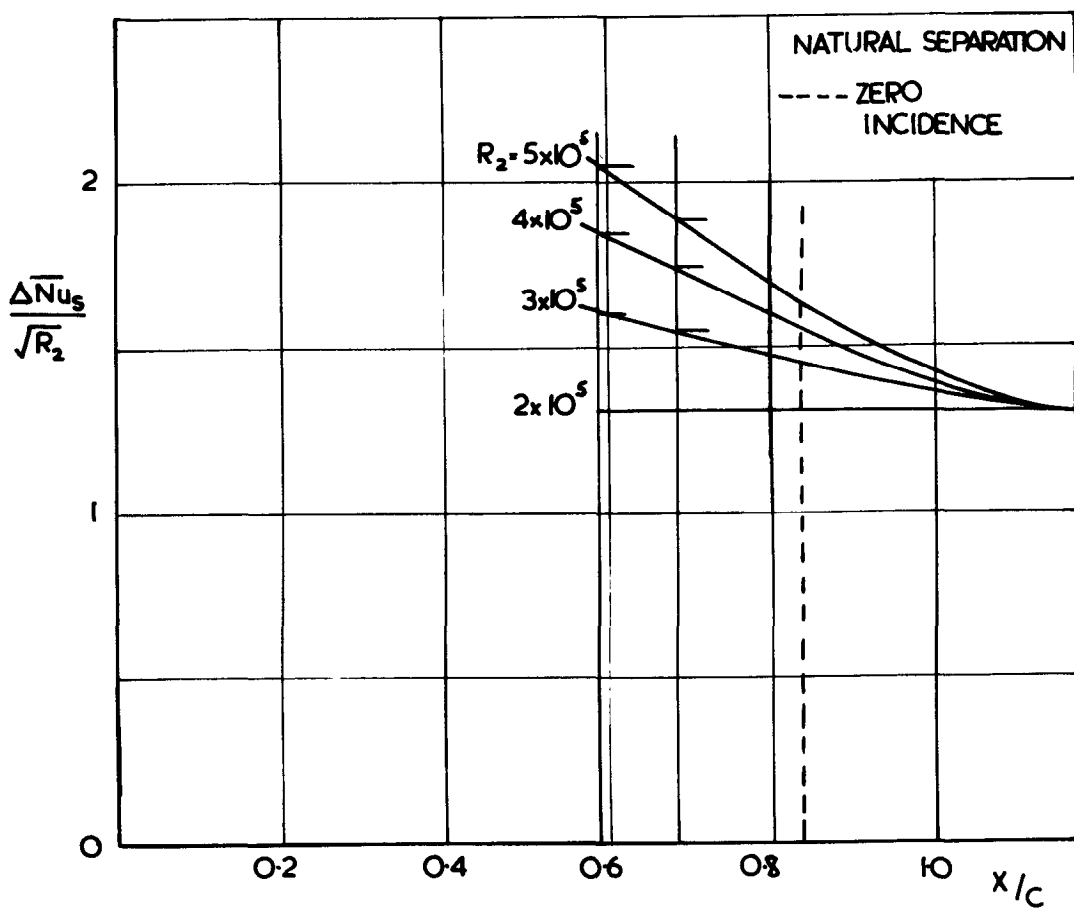
BLOCK HEAT TRANSFER COEFFICIENTS UNDER
SEPARATED FLOW

FIG. 15.
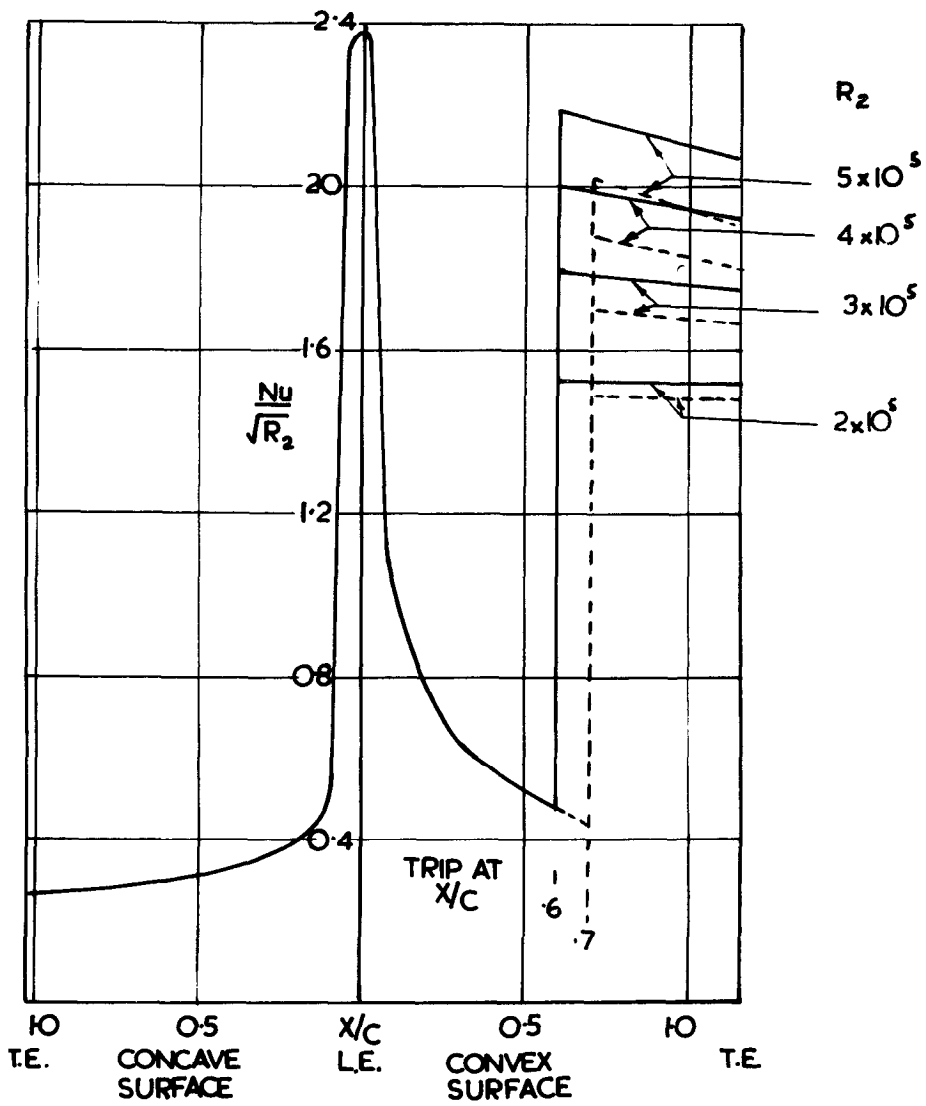
ESTIMATED HEAT TRANSFER
WITH FORCED SEPARATION

FIG.16
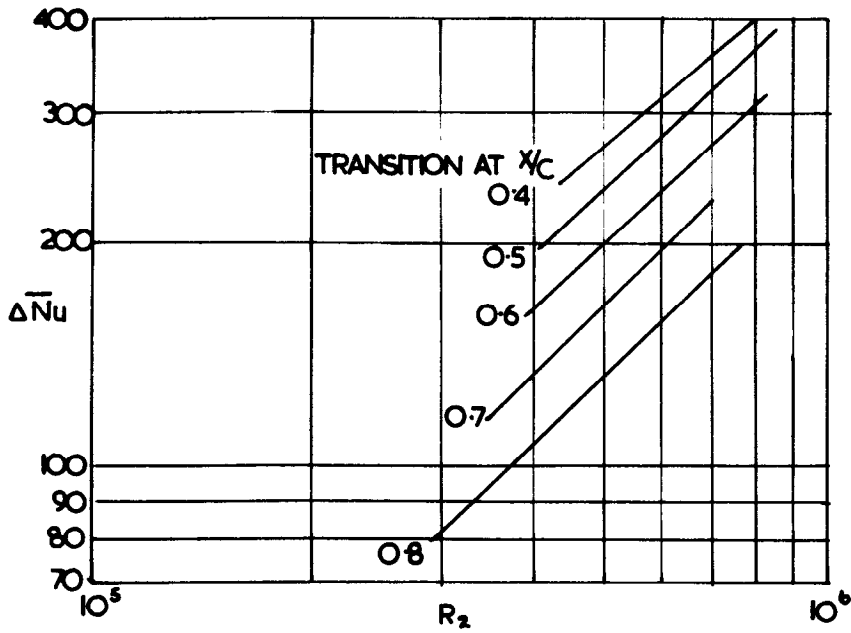
a) TRANSITION ON CONVEX SURFACE
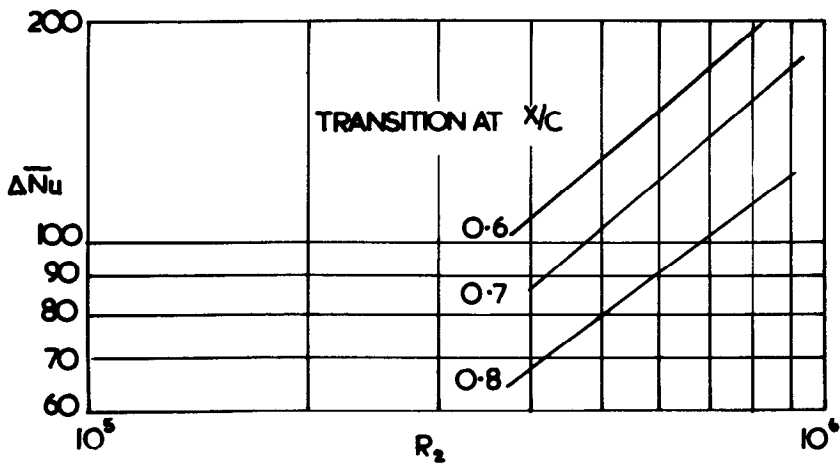
b) TRANSITION ON CONCAVE SURFACE
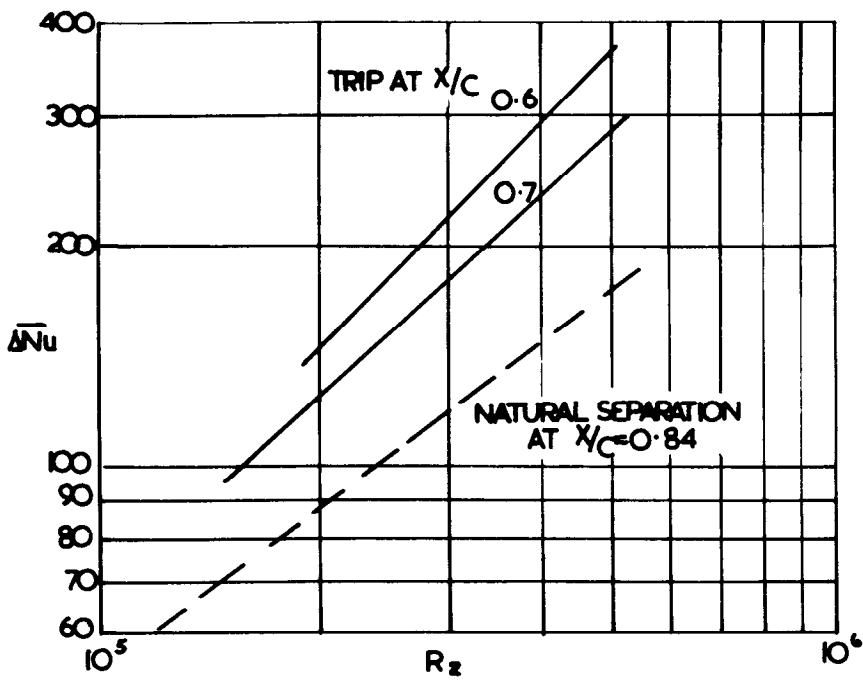
c) SEPARATION ON CONVEX SURFACE

BLADE AVERAGE HEAT TRANSFER INCREMENTS

FIG. 17.
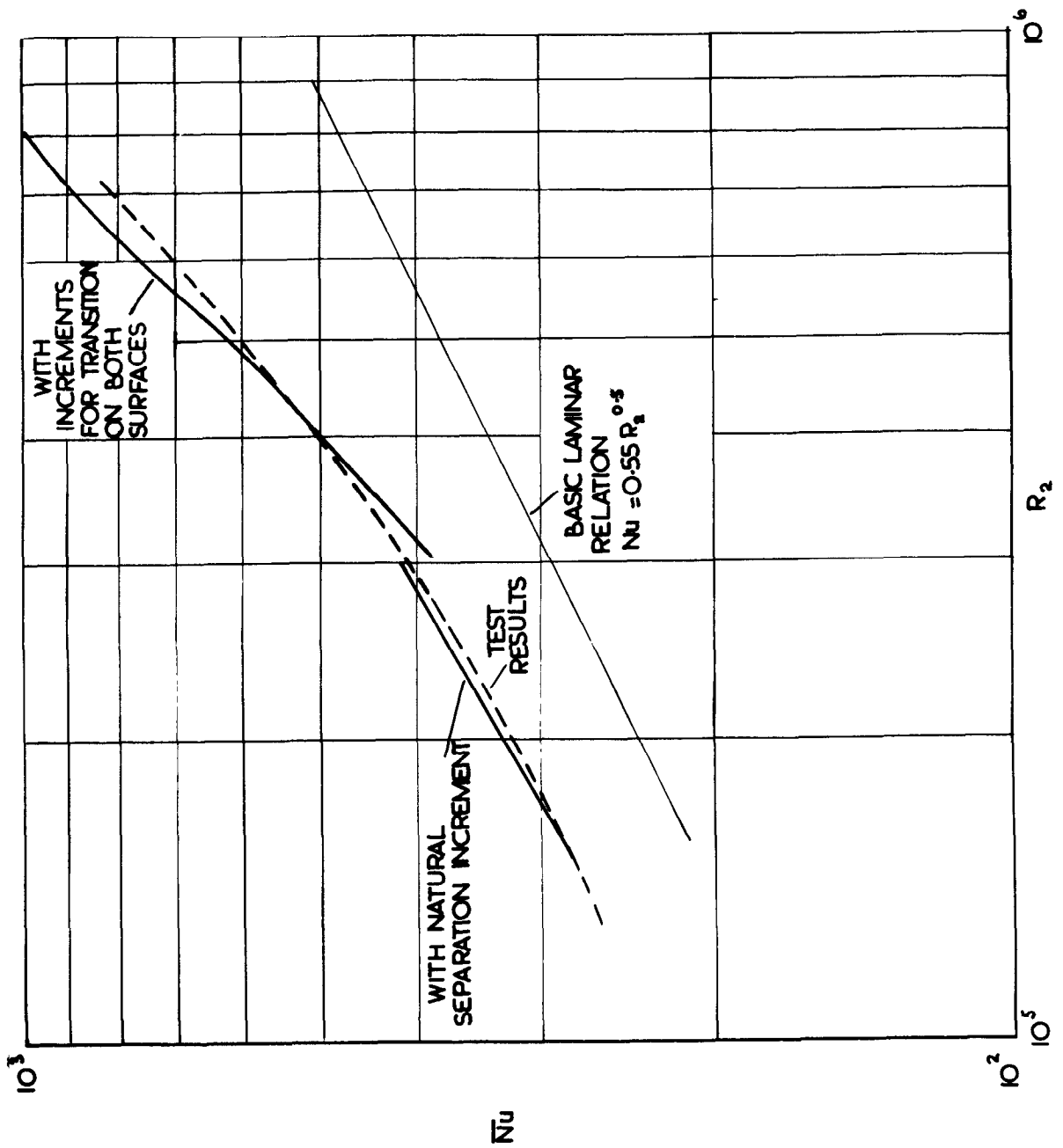
ESTIMATED AND TEST VALUES OF AVERAGE
HEAT TRANSFER

FIG. 18.

CASCADE INLET TURBULENCE LEVELS